Received April 16, 2019, accepted May 7, 2019, date of publication May 14, 2019, date of current version May 31, 2019.

Digital Object Identifier 10.1109/ACCESS.2019.2916882

A Convoluted Frequency Selective Surface for Wideband Communication Applications

SHAHID HABIB[1], GHAFFER IQBAL KIANI[2], AND MUHAMMAD FASIH UDDIN BUTT[1]
[1]Department of Electrical and Computer Engineering, COMSATS University Islamabad, Islamabad 45550, Pakistan
[2]Department of Electrical and Computer Engineering, King Abdulaziz University, Jeddah 21589, Saudi Arabia

Corresponding author: Muhammad Fasih Uddin Butt (fasih@comsats.edu.pk)

This work was supported by the Office of Research, Innovation and Commercialization (ORIC), COMSATS University, under Grant 16-50/CRGP/CIIT/IBD/16/1204.

ABSTRACT A wideband bandstop frequency selective surface (FSS) for electromagnetic interference (EMI) reduction applications is presented for the *S*-, *C*-, and *X*-bands. The proposed FSS is made of convoluted square and circular loop elements, which are employed on the opposite surfaces of the RO3010 substrate. The overall dimensions of the FSS are reduced to 0.15λ at the center frequency compared with the conventional loop elements with an overall decrease in the size of more than 90% at the center frequency. It has a bandwidth of 9 GHz to reduce the harmful effects on the human body due to EMI caused by radio transceivers. It can also be employed as a sub-reflector to enhance the gain and the bandwidth of the antennas. Furthermore, it has many advantages in comparison to the designs presented in the latest research. For example, it has a low profile, the fractional bandwidth is enhanced up to 120%, and it ensures better angular stability for transverse electric (TE) as well as transverse magnetic (TM) polarized waves. Moreover, an average signal attenuation of more than 30.60 and 19.5 dB is ensured in the entire band for TE and TM modes, respectively. The simulation results are obtained using a high-frequency structure simulator (HFSS) and validated through the experimental results.

INDEX TERMS Antennas, angle of incidence, electromagnetic interference, frequency selective surfaces, electromagnetic shielding, shielding effectiveness.

I. INTRODUCTION

FSSs can be constructed by employing the metallic elements of identical geometry on a dielectric substrate or as apertures by perforating a metallic screen in an array of one, two or three dimensions to act as spatial filters for microwave and millimeters wave applications [1]. When an incident electromagnetic wave strikes the FSS, a phenomenon of total transmission or reflection happens to depend upon the geometry of the element. These FSSs are successfully integrated into telecommunications, radomes, antennas, absorbers, wireless security apparatus, missiles, and electromagnetic shielding [1]. Electromagnetic interference (EMI) generated by radio transceivers has become a considerable threat that affects the performance of wireless systems due to electrostatic coupling or electromagnetic induction [2]. Advancement in wireless technology has also affected human health due to the radiation caused by radio devices [3]. Both natural and artificial sources like cellular networks, lightning, Aurora, ignition systems etc. generate variable voltages and currents that may initiate EMI and thus interrupt the operation of a wireless system. To address these challenges many techniques are proposed by different researchers to find out an optimum solution by using FSSs [1], thin metal sheets, such as electromagnetic bandgap structures and metamaterials [4] and [5]. However, FSS has become the most favorite choice due to its several advantages. It can be easily integrated into a wireless system for effective isolation from the interfering signals due to its low profile and lightweight. Another important advantage of FSS is ease in fabrication due to its simple geometry and low cost. In [6], authors have presented an electromagnetic FSS absorber for both high and low permittivity values. They investigated the impact of normal and oblique angles of incidence on the bandwidth of the absorber. The angular and polarization stability were ensured for 0°, 30° and 60° incidence for both TE and TM polarizations. In [7], an FSS based on cantor dust fractal geometry for polarization independent operation for UWB applications was presented. The −10 dB fractional bandwidth of the design was 86.9 % at the center frequency. The angular stability of the proposed FSS was investigated for 0° and 30° incidences. In [8], an FSS of cross-slot element

The associate editor coordinating the review of this manuscript and approving it for publication was Davide Comite.

coated on a flat glass was designed for EMI shielding, for Ku-band applications. The transmission and reflection characteristics were theoretically and experimentally demonstrated for narrow frequency band from 12.2 GHz to 12.7 GHz. However, the aspect of angular and polarization stability was not discussed. Shielding effectiveness for X- and Ka- bands with a −10 dB bandwidth of 7.5 GHz was achieved in [9], using circular and cross-dipole elements. On the basis of the parametric analysis, angular stability of up to 45° incidences was ensured for both polarizations. A multilayer FSS was constructed in [10], using Kotch fractal element with a bandwidth of 6 GHz at −10 dB, where the numerical and experimental results for 0° of incidence were presented. However, due to multilayer geometry, the bottom of the transmission curve is flatter with faster roll-off. A UWB FSS using dual layer metallic structures array operating from 2.87 GHz to 10.87 GHz was designed in [11]. At the center frequency, 8 GHz bandwidth was achieved for TE polarization with fractional bandwidth of 116 %. The paper presented the theoretical and experimental results for normal angle of incidence for TM polarization. A synthesis technique to design a square and modified circular loop FSS having narrow bandwidth was presented in [12]–[13] for satellite communication applications. Researchers in [14]–[20] presented various bandstop FSS for narrow and wideband communication applications. A dual layer wideband stop FSS and its equivalent model was proposed in [15], which solved the synthesis problem in order to acquire the structural parameters of the FSS for the desired frequency band. FSS for X-band shielding applications were proposed by [14] and [18], which investigated the angular and polarization stability up to 60° and 45° incidences, respectively. In [16], a single layer multiband bandstop FSS was designed for WLAN, X-band and WiMAX applications for vertical and horizontal polarization of up to 50° incidences. A bandstop FSS of high and low permittivity values was presented in [19] and [20] having a bandwidth of 1.5 GHz and 2.41 GHz, respectively designed for shielding applications. Convoluted FSS and its advantages over the conventional elements was investigated in [17] for normal angle of incidence. Although several unique aspects were presented in [4]–[17], [17]–[20] and [27] for narrow and wideband communication applications but in all these cases some important features such as angular and polarization stability, transmission curve of extended bandwidth having faster roll-off and flatter bottom, smaller thickness and periodicity of the unit cell and simple geometry of the design were not investigated, as summarized below:

- Angular and polarization stability of the design in [7], [9], [11], and [14]–[17], [17]–[20] were not realized for TE and TM polarization for a higher angle of incidence.
- The −10 dB fractional bandwidth obtained in [7], [9], [14]–[16] and [18]–[20] are narrower.
- The thickness of certain FSSs presented in the literature [7], [9], [15], [16], [19] and [20] are higher and thus increased the overall density and complexity of the respective designs.
- Improper selection of the substrates and elements in [9], [11] and [14]–[19] increased the periodicity of the unit cell which affected the angular and polarization stability of the respective designs.
- To obtain the shielding effectiveness, absorber designs having complex geometries were proposed by different researchers in [4]–[7], [10], [11], [17], [19], [20] and [27].

In this research, a wideband FSS has been designed using convoluted square loop (CSL) and convoluted circular loop (CCL) elements. The U-shaped bending has been introduced at the interval of 90° to the conventional square and circular loop elements. This novelty of convoluting the circular and square elements at the same angle and employing them on the opposite surfaces has resulted in a compact, miniaturized, lightweight and low profile dual-layer wideband FSS as compared to the conventional square and circular loop FSS. Such a compact dual layer FSS design has not been reported to date in which a comprehensive package of wider bandwidth up to 9 GHz, angular and polarization stability up to 80 degrees, shielding effectiveness of more than 19.5 dB and fractional bandwidth of 120% is achieved. The periodicity and dimensions of both square and circular loop elements are kept smaller to remove the grating lobes and to enhance the polarization and angular stability of the wideband convoluted FSS. The FSS dimensions are reduced to 0.15λ at the center frequency with reduction of more than 90% in the size at center frequency 7.5 GHz. Besides the fact that the proposed FSS can be used to increase the performance of radio devices by reducing the EMI as demonstrated in [21]. It can also be employed to improve the gain, bandwidth, directivity, and VSWR of wideband antennas by reflecting the incident waves and thus return loss is also minimized as reported in [22]–[24]. The paper is structured as follows. Geometry, design and dimensions of the FSS are presented in Section II. In Section III, theoretical and experimental results are presented. The section also details the fabrication and experimental setup to verify the simulated results. Shielding effectiveness, angular as well as polarization stability of convoluted FSS is presented in Section IV and V, respectively. Finally, paper is concluded in Section VI.

II. WIDEBAND FSS DESIGN

The dimensions of the designed wideband convoluted FSS are depicted in Fig. 1 and Fig. 2. The convoluted FSS is constructed by CSL and CCL elements employed on the outer surfaces of the substrate. The U-shaped inward bending in the unit cell is introduced at an angle of 0°, 90°, 180° and 270° for both CSL and CCL elements. Bandwidth of the FSS is proportional to the width of the element but at the cost of angular and polarization stability. The width of CSL and CCL elements is optimized and U-shaped bending is introduced as shown in Fig. 1 to improve the angular and polarization stability to achieve a constant bandwidth for TE and TM polarization against normal and oblique angle of incidence. Fig. 1(c) shows the parameters R_1 and R_2 which

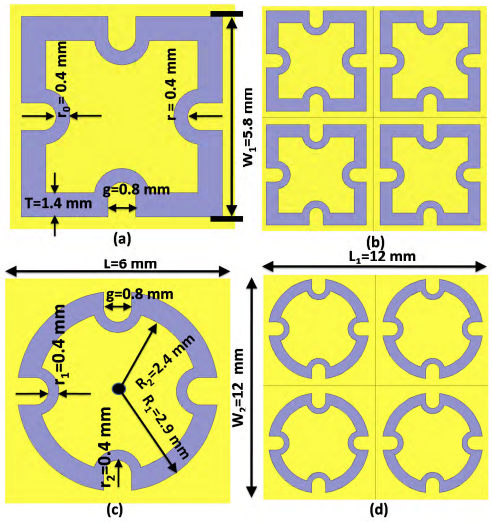

FIGURE 1. Geometry of convoluted CSL and CCL element. (a) The top layer of unit cell CSL element. (b) 2 × 2 periodic array of CSL element. (c) The bottom layer of unit cell CCL element. (d) 2 × 2 periodic array of CCL element.

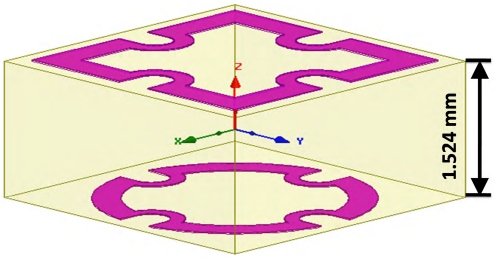

FIGURE 2. 3D view of top and bottom layer of the proposed FSS.

represent the inner and the outer radius of the CCL element, respectively. Fig 1(c) shows the periodicity of CSL and CCL unit cell which is represented by the parameter L. The outer length of CSL element is represented by a parameter W_1 whereas T represents the strip width as shown in Fig. 1(a). The inter-element spacing between CSL and CCL is 0.4 mm in horizontal as well as vertical directions. The 3D view of the designed wideband FSS in Fig. 2 is also showing the thickness of convoluted unit cell that is 1.524 mm. The loss tangent and permittivity of the substrate are 0.02 and 10, respectively. Both the elements are electric conductors which are made of copper having thickness of 0.035 mm. The length and the radius of CSL and CCL elements are calculated as per the following equations, respectively.

$$L \approx \frac{c}{4 \times f_0 \times \sqrt{\varepsilon_{eff}}} \tag{1}$$

$$R \approx \frac{c}{2 \times \pi \times f_0 \times \sqrt{\varepsilon_{eff}}} \tag{2}$$

In the above equations, L is the length of the CSL element. Inner radius of the CCL element is represented by R, c represents the speed of light, ε_r is the permittivity of substrate and ε_{eff} is equal to $(1 + \varepsilon_r)/2$ as suggested in [1]. However, both the equations give the approximated values which are further optimized by adjusting the values of different parameters of

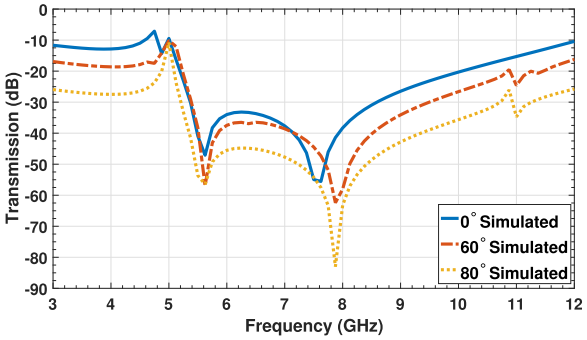

FIGURE 3. Simulation results of dual layer conventional FSS for TE polarization at 0°, 60° and 80° incidence.

the proposed wideband convoluted FSS. Finally, the thickness of the proposed design has been adjusted to make it compact and low-profile according to the following parameters suggested in [1]:

- Firstly, RO3010 having high permittivity (ε_r) value has been used to reduce the thickness of the substrate as suggested in [1]. Both lower (f_l) and higher (f_h) resonance frequencies are adjusted between $[f_l / \sqrt{\varepsilon_r}, f_l]$ and $[f_h / \sqrt{\varepsilon_r}, f_h]$, respectively.
- Secondly, thickness *(d)* of the substrate has been optimized by using the relation indicated in [1]. The guided wavelength (λ_ε) is calculated using the following formula:

$$\lambda_\varepsilon = \frac{\lambda_0}{\sqrt{\varepsilon_{eff}}}, \tag{3}$$

where λ_0 is the operating wavelength which satisfies the thickness parameter of the proposed FSS. Thus, high permittivity value of a dielectric substrate will reduce the guided wavelength which will further reduce the thickness of the substrate. However, a high permittivity material decreases the bandwidth of the FSS as mentioned in [1]. This bandwidth-thickness dilemma has been addressed in this work by using the dual layer FSS based on convoluted loop elements, which results in wider bandwidth of 9 GHz for TE and TM polarizations up to 80 degree incidence, as demonstrated in Section III.

III. THEORETICAL AND EXPERIMENTAL RESULTS

The modeling and simulation are done in ANSYS HFSS [25] using master and slave boundaries with two Floquet ports. The structure is excited with the plane waves through Floquet ports then transmission and reflection coefficients are calculated in terms of S-parameters. Firstly, conventional square and circular loop elements of the same dimensions of CSL and CCL are simulated without introducing U-shaped inward bending to investigate the difference between the conventional and convoluted square and circular based FSS. For conventional square and circular elements resonance frequencies are significantly shifted across at 60° and 80° incidence for TE and TM polarizations. Thus, overall bandwidth and angular stability is affected as shown in Fig. 3 and Fig. 4.

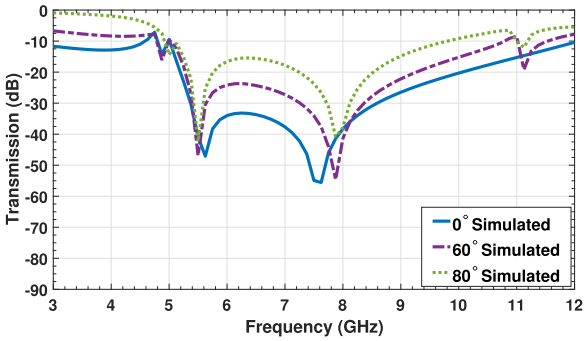

FIGURE 4. Simulation results of dual layer conventional FSS for TM polarization at 0°, 60° and 80° incidence.

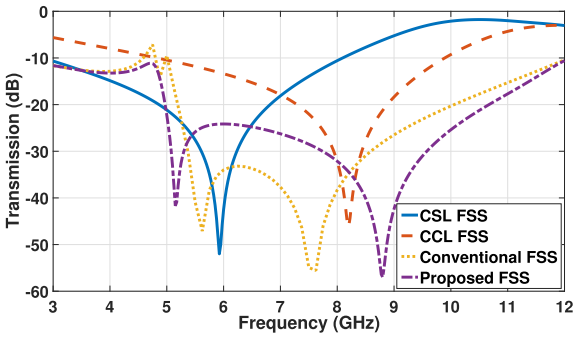

FIGURE 5. Simulation results at 0° for CSL, CCL, conventional and the proposed FSS.

It can also be noticed that some grating lobes around 4.8 GHz and 11 GHz are observed for both polarizations. Secondly, CCL and CSL elements are designed and simulated separately to resonate at lower and higher frequencies, respectively. A comparison of conventional and convoluted FSS is presented in Table 1. It has been observed that bandstop characteristics have been significantly enhanced by introducing U-shaped bending in conventional square and circular loop elements. U-shaped bending in conventional loop elements has many advantages over the conventional loop elements such as reduction in the overall size of the unit cell; elimination of grating effects; minimization of loading of elements; increase in angular and polarization stability and a stable bandwidth of FSS at -10 dB for normal and higher angles of incidence. Simulation results of CSL, CCL, conventional and the proposed FSS at 0° can be seen in Fig. 5. For CSL, the resonance frequency is 5.87 GHz at normal incidence with the transmission coefficient of -51.99 dB having 5.15 GHz bandwidth at -10 dB. The results show a resonance frequency of 8.2 GHz for CCL FSS having a transmission coefficient of -46.22 dB with a bandwidth of 5.10 GHz at -10 dB. For conventional FSS, f_l and f_h frequencies are 5.8 GHz and 7.6 GHz with the transmission coefficient of -47.90 dB and -55.80 dB, respectively and offering bandwidth of 7 GHz at -10 dB. Finally, CSL and CCL elements are employed on the outer surfaces of the substrate to get the wider bandwidth of 9 GHz as observed in Fig. 5. Table 2 summarizes -10 dB bandwidth for TE and TM polarized waves at 0°, 60° and 80°. The lower and upper resonance frequencies along with the transmission coefficients are also presented in Table 2. For TE polarized wave a bandwidth of 9 GHz is achieved at 0°, 60° and 80° incidence. For TM polarization the bandwidth of 9 GHz is achieved at 0° and 60° incidence whereas at 80° bandwidth has been reduced to 5 GHz. To endorse the simulated results, a prototype of 29 × 41 cells of 178 × 228 mm^2 dimensions was fabricated using RO3010 of 1.524 mm thickness with $\varepsilon_r = 10$ as shown in Fig. 6. Network analyzer from Agilent Technologies PNA-X N5242A [26], with two 15 dBi horn antennas, having operating bandwidth 10 MHz to 26.5 GHz and 1 GHz to 18 GHz, respectively are utilized. The perspective view of free space experimental setup can be seen in Fig. 7. For free space measurements, aluminum shielding screen is integrated with the stand to restrict the transmission of signals. The stand is placed between the transmitting (T_x) and receiving (R_x) antennas, as shown in Fig. 7. The prototype is placed in the stand of aluminum shielding screen. It is ensured that there is no leakage of signals between the boundaries of prototype and aluminum shielding screen during the measurement. Before the measurements of FSS, calibration of the experimental setup was conducted through the open window of aluminum shielding screen and free space propagation loss is measured which is later subtracted from the FSS measurements to eliminate the impact of attenuated microwave signals. The space between the T_x and R_x antennas has been calculated using the far-field theorem as per the below equation.

TABLE 1. Comparison between conventional and wideband convoluted FSS for TE and TM polarizations at 0°, 60° and 80° angle of incidence for -10 dB transmission.

Polarization and angle of incidence	Average S_{12} of Conventional FSS	Bandwidth of Conventional FSS	Average S_{12} of Proposed FSS	Bandwidth of Proposed FSS
TE 0°	-21.47 (dB)	7.00 (GHz)	-24.96 (dB)	9 (GHz)
TE 60°	-27.57 (dB)	7.00 (GHz)	-30.45 (dB)	9 (GHz)
TE 80°	-37.44 (dB)	7.00 (GHz)	-38.91 (dB)	9 (GHz)
TM 0°	-21.47 (dB)	7.00 (GHz)	-24.96 (dB)	9 (GHz)
TM 60°	-18.2 (dB)	7.00 (GHz)	-22.94 (dB)	9 (GHz)
TM 80°	-11.03 (dB)	4.5 (GHz)	-13.31 (dB)	5 (GHz)

TABLE 2. −10 dB transmission of wideband convoluted FSS for TE and TM polarizations at 0°, 60° and 80° angle of incidence.

Polarization and angle of incidence	Lower resonance frequency/S_{12}	Higher resonance frequency/S_{12}	Bandwidth
TE 0°	5.15 (GHz) /-38.70 (dB)	8.80 (GHz) /-54.99 (dB)	9 (GHz)
TE 60°	5.17 (GHz) /-45.83 (dB)	8.77 (GHz) /-65.34 (dB)	9 (GHz)
TE 80°	5.20 (GHz) /-57.83 (dB)	8.87 (GHz) /-67.78 (dB)	9 (GHz)
TM 0°	5.15 (GHz) /-38.70 (dB)	8.80 (GHz) /-54.99 (dB)	9 (GHz)
TM 60°	5.30 (GHz) /-41.35 (dB)	8.95 (GHz) /-52.30 (dB)	9 (GHz)
TM 80°	5.5 (GHz) /-42.37 (dB)	7.90 (GHz) /-47.39 (dB)	5 (GHz)

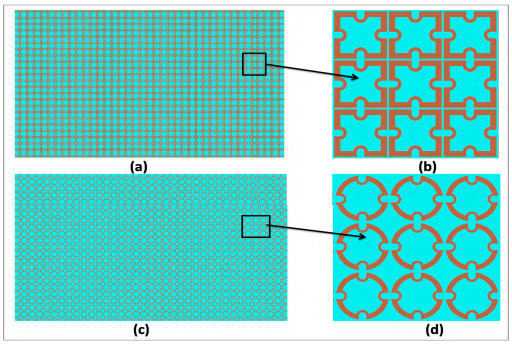

FIGURE 6. Fabricated FSS on RO3010. (a) Top layer of prototype. (b) 3 × 3 fabricated cells of the top layer. (c) Bottom layer of prototype. (d) 3 × 3 fabricated cells of the bottom layer.

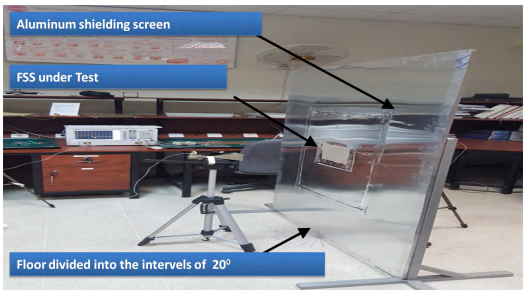

FIGURE 7. Perspective view of free space experimental setup.

$$d_{farfield} \geq \frac{2D^2}{\lambda} \tag{4}$$

where $d_{farfield}$ is the distance between the two horn antennas which is 600 mm. λ and D are representing the wavelength at the center frequency and the maximum dimension of T_x and R_x antennas, respectively. To measure the transmission through FSS at 0°, 60° and 80° angle of incidence the floor is divided into the two equal parts of cartesian coordinates. Both the parts are equally divided into the intervals of 150. To measure the transmission through FSS at 0° both T_x and R_x antennas are placed at an angle of 90° in relation to the FSS under test. The center of the aluminum shielding stand is placed at the origin where both $x = 0$ and $y = 0$ facing T_x and R_x antennas. Aluminum shielding screen stand is manually rotated at the line of 60° and 80° to quantify the transmission through the proposed FSS at 60° and 80° angle of incidence. The procedure to measure the magnitude of the transmission through the FSS is the same for TE and TM polarizations except that both the antennas are only rotated by an angle of 90° for TM modes. Experimental and simulated results of proposed FSS at 0°, 60° and 80° incidence are plotted in Fig. 8 and Fig. 9 for both the polarizations. The lower resonance frequency is 5.15 GHz whereas higher resonance frequency is 8.8 GHz, while their corresponding transmission coefficients are −38.70 dB and −54.99 dB, respectively. It is observed that a stopband of wider bandwidth of 9 GHz achieved at −10 dB, when both elements are placed on the outer sides of the substrate. It is also noticed that for convoluted FSS, due to mutual coupling of CSL and CCL elements, resonance frequencies at 0°, 60° and 80° are shifted across from 5.92 GHz to 5.15 GHz and 8.2 GHz to 8.8 GHz which resulted in wider bandwidth. It is apparent that for the designed FSS there is a great agreement among the experimental and simulated results. Table 3 compares some important aspects of different designs which are published in the literature. In the literature, researchers have presented −10 dB bandwidth (BW) and fractional bandwidth (FBW) against their proposed design for wideband communication applications using the following equations:

$$BW(GHz) = f_H - f_L \tag{5}$$

$$FBW(\%) = \frac{BW}{f_c} \times 100 \tag{6}$$

In above equations f_H, f_L and f_c are the higher, lower and center frequencies. Using the above equations, we have calculated −10 dB bandwidth and fractional bandwidth for the proposed FSS which is presented in Table 3. In [7], [9], [11] and [15] −10 dB bandwidth are 8 GHz, 7.50 GHz, 8 GHz and 8 GHz, respectively. But these bandwidths were obtained at the cost of size, angular and polarization stability, shielding effectiveness, fractional bandwidth and higher substrate thickness, as shown in Table 3. In this work, as compared to various FSSs presented in other research works, bandwidth is extended to 9 GHz for both polarizations, angular stability is ensured up to 80°, fractional bandwidth is enhanced to 120%, the thickness and size of the unit cell is significantly minimized as illustrated in Table 3. A significant reduction in size was achieved by introducing U-shaped bending in a conventional FSS which has minimized the periodicity of unit cell along x- and y- directions and thereby the performance of the proposed FSS has significantly improved as compared to the conventional FSS. The overall size of the wideband convoluted FSS is reduced about 75%, 98%, 22%, 22%, 64% and 36% as compared to [9], [13], [14], [15], [17] and [18], respectively as established in [27]. The magnitude of electric

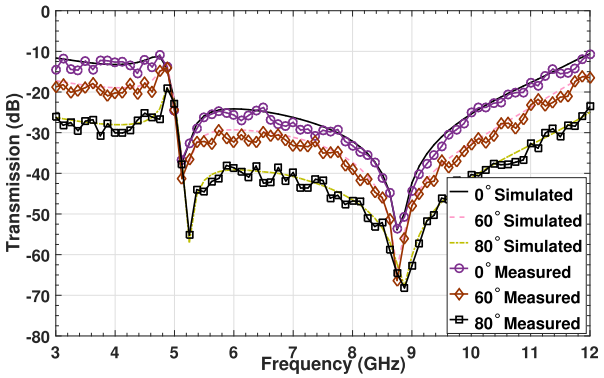

FIGURE 8. Simulation and measured results of the proposed wideband convoluted FSS for TE polarization at 0°, 60° and 80° angle of incidence.

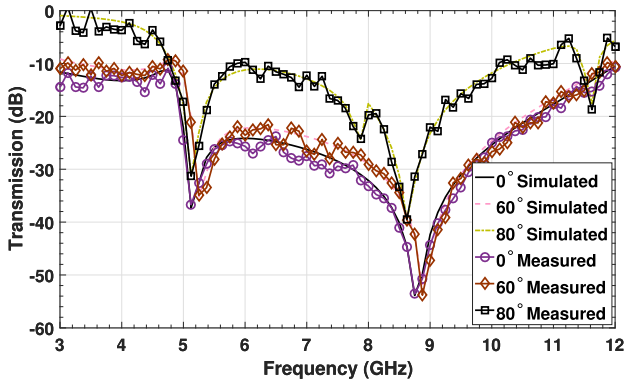

FIGURE 9. Simulation and measured results of the proposed wideband convoluted FSS for TM polarization at 0°, 60° and 80° angle of incidence.

field on the surface of the proposed FSS are demonstrated in Fig. 10. To understand the physics of the proposed FSS, convoluted unit cell is excited by a horizontally and vertically polarized wave along z^+ direction. Higher surface current density against lower and higher resonance frequencies is demonstrating the reflection characteristics of the incident electric (E_i) wave along z^+ direction. It can be observed in Fig. 10 (b), Fig. 10 (c) and Fig. 10 (d) that the surface current density is greater at 5.17 GHz, 7.50 GHz and 8.77 GHz, thus demonstrating the existence of stopband at lower, central and higher resonance frequencies, respectively. For out of stopband at 1 GHz the surface current density is lesser which can be shown in Fig. 10 (a), as an incident wave transmits through the proposed FSS which results in higher transmission coefficients.

IV. SHIELDING EFFECTIVENESS

Performance of the proposed FSS is analyzed through shielding effectiveness which can be calculated using the following relation given in [9]

$$S(dB) = 20 \times log|\frac{E_i}{E_t}| \tag{7}$$

In the above equation, E_i and E_t are incident and transmitted electric field component, respectively. It can be observed in Fig. 11 and Fig. 12 that an average attenuation of 30.60 dB and 19.57 dB for TE as well as TM polarizations is achieved, respectively from 3 GHz to 12 GHz against 0°, 60° and 80° incidence.

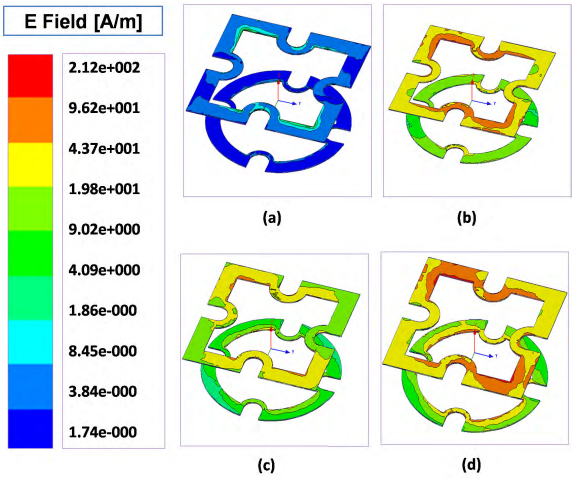

FIGURE 10. Electric field distribution on the surface of the proposed wideband convoluted FSS. (a) 1.00 GHz. (b) 5.15 GHz. (c) 7.50 GHz. (d) 8.77 GHz.

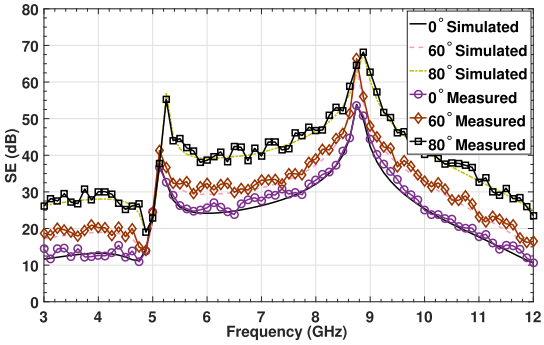

FIGURE 11. Simulation and measured shielding effectiveness of the proposed wideband convoluted FSS for TE polarization at 0°, 60° and 80° angle of incidence.

V. ANGULAR AND POLARIZATION STABILITY

Theoretical and experimental results for both vertically and horizontally polarized waves are presented for 0°, 60° and 80° angles of incidence. Angular as well as polarization stability of the wideband convoluted FSS is ensured up to 80° and 60° for TE and TM modes, respectively which could not be achieved in [7]–[11], [15], [18] and [20]. Loop elements are selected to pack them closer together to reduce the inter-element spacing which resulted in greater bandwidth, better resonance stability for normal and oblique angle of incidence.

In this work, angular stability is achieved because of least inter-element spacing, U-shaped bending and appropriate dimensions of the overall FSS structure. U-shaped bending is introduced for angular and polarization stability in [17] and [18] to achieve the wider bandwidth, shielding effectiveness and to lessen the overall size of the FSS. The flatness of the transmission curve is also achieved by placing a dielectric slab between the CSL and CCL elements as suggested in [1]. The dimension and periodicity along x and y directions is 0.15λ at the center frequency which is 3.12 times less than the operating frequency at 3 GHz. The thickness of the substrate is $\lambda/26$ which is also smaller than $\lambda/4$ at the center frequency as compared to the conventional multi-layer FSS [11], thus

TABLE 3. Comparison of various FSS reported in the literature.

Reference	Bandwidth (GHz)	Fractional Bandwidth (%)	Angular Stability	Thickness (mm)	Periodicity (mm)	Size (mm^2)
[7]	8.00	80.00	30°	–	–	–
[9]	7.50	73.17	45°	3.20	12.0	144.00
[11]	8.00	114.00	0°	1.80	16.0	256.00
[14]	4.00	48.00	60°	0.13	6.8	46.24
[15]	8.00	89.00	0°	3.00	6.8	46.24
[16]	4.00	48.00	60°	1.60	10.0	100.00
[17]	6.50	120.00	50°	1.60	10.0	100.00
[18]	4.00	48.00	45°	0.13	7.5	56.25
[19]	1.50	40.00	75°	2.00	3.0	9.00
[20]	2.41	28.57	0°	7.75	10.0	100.00
[***This work***]	9.00	120.00	80°	1.52	6.0	36.00

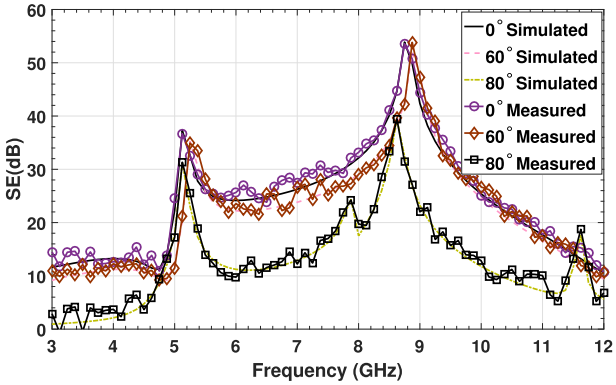

FIGURE 12. Simulation and measured shielding effectiveness of the proposed wideband convoluted FSS for TM polarization at 0°, 60° and 80° angle of incidence.

making it low profile. No grating lobe was observed due to the smaller inter-element spacing making the FSS more stable for both the polarized waves at normal and higher angle of incidence. As observed, proposed FSS has ensured angular stability for large angle of incidence. At normal angle of incidence the transmission coefficients are identical for both the polarizations, since the structure of the FSS is symmetrical. However, it is noticed that the bandstop characteristics of the FSS are altered for both the polarizations as the angle of incidence is increased. The bandwidth for TE polarization is extended whereas bandwidth for TM polarization is degraded as the angle of incidence is increased. The bandwidth of the proposed wideband FSS is constant for TE and TM modes up to 60°. But at 80° angle of incidence, its bandwidth is reduced for TM polarization from 9 GHz to 5 GHz. This degradation in the bandwidth was experienced due to the variation in the wave impedance for both the polarizations as demonstrated in [28]–[33]. For TE mode wave impedance decreases as the angle of incidence increases resulting in smaller quality factor that leads to a greater fractional bandwidth. For TM mode, the wave impendence is increased by increasing the angle of incidence. Thus, quality factor is increased that causes a smaller bandwidth for TM polarization.

VI. CONCLUSION

A low profile, lightweight, wideband FSS is proposed which is validated through simulation and experimental results. Good angular and polarization stability are achieved for a bandwidth of 9 GHz. It covers S, C, and X bands and provides an average SE of more than 20 dB. The same design can be utilized for Ku, Ka, and K bands by optimizing the dimensions of the proposed FSS using equations 1 and 2. The proposed design has minimized the overall size to more than 90% as compared to the corresponding conventional loop elements. The FSS design can have numerous applications such as gain and bandwidth enhancement in antennas due to its reflection characteristics. Performance of radio devices can be enhanced by reducing EMI with the help of the proposed FSS. It can also be utilized for EMI suppression in aerospace systems as well as in military ground vehicles for their mobile communication. Moreover, it can be used for WLAN security for 3.6 GHz, 4.9 GHz, 5 GHz and 6 GHz frequency bands. For the indoor environment, a no signal zone can be created by placing the convoluted FSS at the entrance of the unwanted signals to reduce the harmful effects of EM waves on the human body.

REFERENCES

[1] B. A. Munk, *Frequency Selective Surfaces: Theory and Design*, 2nd ed. New York, NY, USA: Wiley, 2000.
[2] A. I. Zverev, *Handbook of Filter Synthesis*. New York, NY, USA: Wiley, 1967.
[3] R. S. A. Larik, G. A. Mallah, M. M. A. Talpur, A. K. Suhag, and F. A. Larik, "Effects of wireless devices on human body," *J. Comput. Sci. Syst. Biol.*, vol. 9, pp. 119–124, Jan. 2016.
[4] D. Seetharamdoo, M. Berbineau, A.-C. Tarot, and K. Mahdjoubi, "Evaluating the potential shielding properties of periodic metamaterial slabs," in *Proc. Int. Symp. Electromagn. Compat.-EMC Europe*, Athens, Greecen, Jun. 2009, pp. 1–4.
[5] D. Sievenpiper, L. Zhang, R. F. J. Broas, N. G. Alexopolous, and E. Yablonovitch, "High-impedance electromagnetic surfaces with a forbidden frequency band," *IEEE Trans. Microw. Theory Techn.*, vol. 48, no. 11, pp. 2059–2074, Nov. 1999.
[6] O. Luukkonen, F. Costa, C. R. Simovski, A. Monorchio, and S. A. Tretyakov, "A thin electromagnetic absorber for wide incidence angles and both polarizations," *IEEE Trans. Antennas Propag.*, vol. 57, no. 10, pp. 3119–3125, Oct. 2009.

[7] F. C. G. da Silva Segundo, A. L. P. S. Campos, and E. C. Braz, "Wide band frequency selective surface for angular and polarization independent operation," *Microw. Opt. Technol. Lett.*, vol. 57, no. 1, pp. 216–219, Jan. 2014.
[8] H.-Y. Chen and Y.-K. Chou, "An EMI shielding FSS for Ku-band applications," in *Proc. IEEE Int. Symp. Antennas Propag.*, Chicago, IL, USA, Jul. 2012, pp. 1–2.
[9] I. S. Syed, Y. Ranga, L. Matekovits, K. P. Esselle, and S. G. Hay, "A single-layer frequency-selective surface for ultrawideband electromagnetic shielding," *IEEE Trans. Electromagn. Compat.*, vol. 56, no. 6, pp. 1404–1411, Dec. 2014.
[10] R. H. C. Maniçoba, A. G. d'Assunção, and A. L. P. S. Campos, "Wide stopband cascaded frequency selective surfaces with Koch fractal elements," *Dig. 14th Biennial IEEE Conf. Electromagn. Field Comput.*, Chicago, IL, USA, May 2012, p. 1.
[11] N. Kushwaha, R. Kumar, R. V. S. R. Krishna, and T. Oli, "Design and analysis of new compact UWB frequency selective," *Prog. Electromagn. Res. C*, vol. 46, pp. 31–39, Jan. 2014.
[12] K. R. Jha, G. Singh, and R. Jyoti, "A simple synthesis technique of single-square-loop frequency selective surface," *Prog. Electromagn. Res. B*, vol. 45, pp. 165–185, Jan. 2012.
[13] G. Bharti, K. R. Jha, G. Singh, and R. Jyoti, "Design of angular and polarization stable modified circular ring frequency selective surface for satellite communication system," *Int. J. Microw. Wireless Technol.*, vol. 8, pp. 899–907, Mar. 2015.
[14] M. Nauman, R. Saleem, A. K. Rashid, and M. F. Shafique, "A miniaturized flexible frequency selective surface for X-band applications," *IEEE Trans. Electromagn. Compat.*, vol. 58, no. 2, pp. 419–428, Apr. 2016.
[15] N. Liu, X. Sheng, C. Zhang, J. Fan, and D. Guo, "A design method for synthesizing wideband band-stop FSS via its equivalent circuit model," *IEEE Antennas Wireless Propag. Lett.*, vol. 16, pp. 2721–2725, Aug. 2017.
[16] M. Bashiri, C. Ghobadi, J. Nourinia, and M. Majidzade, "WiMAX, WLAN, and X-band filtering mechanism: Simple-structured triple-band frequency selective surface," *IEEE Antennas Wireless Propag. Lett.*, vol. 16, pp. 3245–3248, Nov. 2017.
[17] E. A. Parker and A. N. A. El Sheikh, "Convoluted array elements and reduced size unit cells for frequency-selective surfaces," *IEE Proc.-H Microw., Antennas Propag.*, vol. 138, no. 1, pp. 19–22, Feb. 1991.
[18] W. Y. Yong *et al.*, "Flexible convoluted ring shaped FSS for X-band screening application," *IEEE Access*, vol. 6, pp. 11657–11665, Mar. 2018.
[19] L. Li *et al.*, "All-dielectric metamaterial frequency selective surfaces based on high-permittivity ceramic resonators," *Appl. Phys. Lett.*, vol. 106, no. 21, pp. 21909–212904, 2015.
[20] F. Yu *et al.*, "Reflective frequency selective surface based on low-permittivity dielectric metamaterials," *Appl. Phys. Lett.*, vol. 107, no. 21, pp. 211906–211910, Nov. 2015.
[21] *Military Applications*. Accessed: Jun. 28, 2018. [Online]. Available: http://www.masttechnologies.com
[22] M. Pasian, S. Monni, A. Neto, M. Ettorre, and G. Gerini, "Frequency selective surfaces for extended bandwidth backing reflector functions," *IEEE Trans. Antennas Propag.*, vol. 58, no. 1, pp. 43–50, Jan. 2010.
[23] Y. Ranga, L. Matekovits, A. R. Welly, and K. P. Esselle, "A constant gain ultra-wideband antenna with a multi-layer frequency selective surface," *Prog. Electromagn. Res. Lett.*, vol. 38, pp. 119–125, Mar. 2013.
[24] F. A. Tahir, T. Arshad, S. Ullah, and J. A. Flint, "A novel FSS for gain enhancement of printed antennas in UWB frequency spectrum," *Microw. Opt. Technol. Lett.*, vol. 59, no. 10, pp. 2698–2704, Jul. 2017.
[25] *3D EM Field Simulator for RF Wireless Design*. Accessed: Jun. 2018. [Online]. Available: http://www.ansys.com
[26] *PN5242A PNA-X Microwave Network Analyzer, 26.5 GHz*. Accessed: Jul. 2018. [Online]. Available: https://www.keysight.com
[27] J.-Y. Xue, S.-X. Gong, W.-Wang, and F.-F. Zhang, "A new miniaturized fractal frequency selective surface with excellent angular stability," *Prog. Electromagn. Res. Lett.*, vol. 13, pp. 131–138, Jan. 2010.
[28] R. Dickie *et al.*, "Submillimeter wave frequency selective surface with polarization independent spectral responses," *IEEE Trans. Antennas Propag.*, vol. 57, no. 7, pp. 1985–1994, Jul. 2009.
[29] Y. Z. Cheng *et al.*, "Ultrabroadband plasmonic absorber for terahertz waves," *Adv. Opt. Mater.*, vol. 3, no. 3, pp. 376–380, 2014.
[30] M. Eular, V. Fusco, R. Cahill, and R. Dickie, "325 GHz single layer sub-millimeter wave FSS based split slot ring linear to circular polarization convertor," *IEEE Trans. Antennas Propag.*, vol. 58, no. 7, pp. 2457–2459, Jul. 2010.
[31] Y. Z. Cheng *et al.*, "Ultrabroadband reflective polarization convertor for terahertz waves," *Appl. Phys. Lett.*, vol. 105, no. 18, Nov. 2014, Art. no. 181111.
[32] N. Behdad, "A second-order band-pass frequency selective surface using nonresonant subwavelength periodic structures," *Microw. Opt. Technol. Lett.*, vol. 50, no. 6, pp. 1639–1643, Jun. 2008.
[33] A. Ebrahimi *et al.*, "Second-order terahertz bandpass frequency selective surface with miniaturized elements," *IEEE Trans. THz Sci. Technol.*, vol. 5, no. 5, pp. 761–769, Sep. 2015.

SHAHID HABIB received the M.Sc. degree in electronics from Quaid-i-Azam University, in 2005, and the M.S. degree in electronic engineering from ISRA University, in 2011. He is currently pursuing the Ph.D. degree in electrical engineering with COMSATS University Islamabad, Pakistan, where he is also an active member of the Next Generation Communications Research Group, Department of Electrical and Computer Engineering. He has more than 12 years of experience in telecommunication industry, and he was a Field Operations Manager and a Specialist. He has published five conference and two journal papers. His research interests include frequency selective surfaces (FSSs), radio-frequency identification (RFID), FPGA-based communication systems design, and optical fiber communication systems..

GHAFFER IQBAL KIANI received the B.Sc. degree (Hons.) in electrical and electronic engineering from the Islamic University of Technology, Dhaka, Bangladesh, in 1997, the M.Sc. degree (Hons.) in electronic engineering from the Ghulam Ishaq Khan (GIK) Institute of Engineering Sciences and Technology, Topi, Pakistan, in 2003, and the Ph.D. degree in electronic engineering from Macquarie University, Sydney, Australia, in 2009. From 2009 to 2012, he was a Postdoctoral Fellow in very-high throughput wireless communication systems at the Commonwealth Scientific and Industrial Research Organization (CSIRO) ICT Centre, Sydney. Since 2013, he has been an Assistant Professor with the Department of Electrical and Computer Engineering, King Abdulaziz University, Jeddah, Saudi Arabia. He has published many high-quality research papers in the field of antennas and propagation. His current research interests include frequency selective surfaces, metamaterials, electromagnetics, antenna design, microwave polarizers, MEMS, NEMS, RFIDs, and THz modulators. He received the Best Student Paper Award from the 2008 Workshop on Applications of Radio Science (WARS) Conference, Gold Coast, Australia, for the paper, Transmission Improvement of Useful Signals through Energy Saving Glass Windows Using Frequency Selective Surfaces.

MUHAMMAD FASIH UDDIN BUTT received the B.E. degree from the National University of Sciences and Technology (NUST), Pakistan, in 1999, the M.E. degree in digital communication/computer networks from the University of Engineering and Technology, Taxila, Pakistan, in 2003, and the Ph.D. degree in electronics and electrical engineering from the School of Electronics and Computer Science, University of Southampton, U.K., in 2010. He is currently a tenured Associate Professor and the Head of the Next Generation Communications Research Group, Department of Electrical and Computer Engineering, COMSATS University Islamabad, Pakistan, where he has been serving as an Academic, since 2002. He has published over 35 research papers in various reputed journals and conference proceedings. His research interests include channel coding, cooperative cognitive radio networks, mm-wave radio-over-fiber technologies, physical-layer security, quantum communications, and frequency selective surfaces.